Supporting Information

Improving uncertainty estimation in urban hydrological modeling by statistically describing bias

Hydrology and Earth System Sciences

D. Del Giudice, M. Honti, A. Scheidegger, C. Albert, P. Reichert, and J. Rieckermann

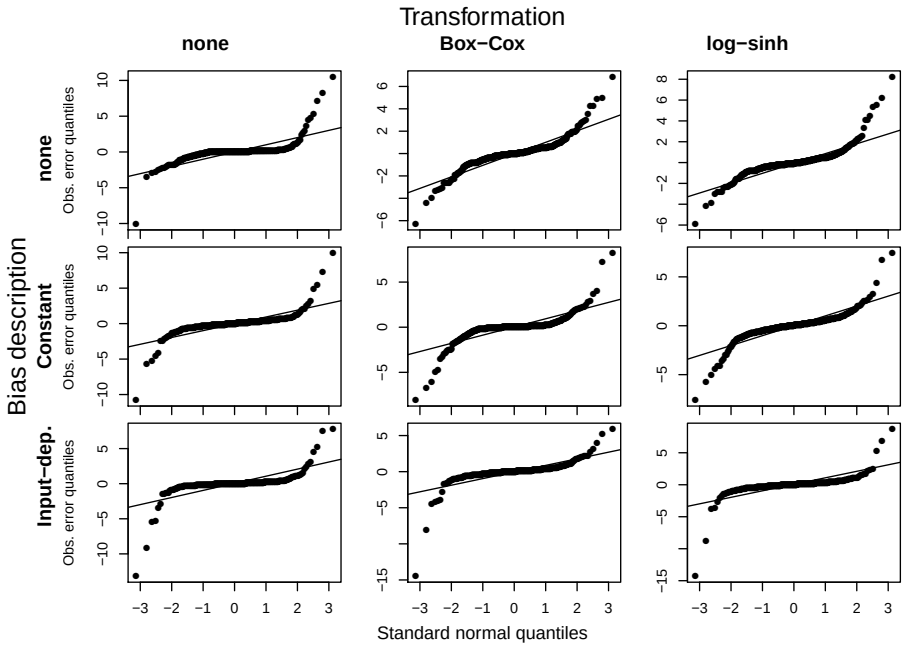

Figure S1: Quantile-Quantile plots for median of **E** (frequentist part of the residuals due to random measurement errors) in the calibration period of 22/23 July.

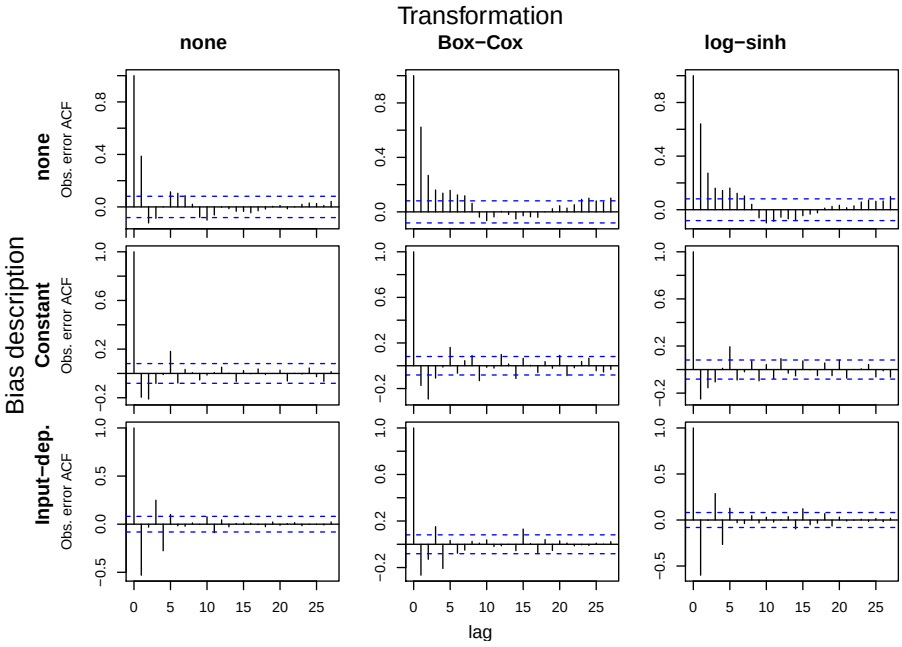

Figure S2: Autocorrelation Function plots for median of **E** (frequentist part of the residuals due to random measurement errors) in the calibration period of 22/23 July.

Table 1: Hydrodynamic model and error model calibration parameters ($\boldsymbol{\theta}, \boldsymbol{\psi}$). The notation for prior distributions is: LN(μ, σ): lognormal, TN(μ, σ, a_1, a_2): truncated normal, Exp(λ^{-1}): exponential. The symbol meaning is: μ: expected value, σ: standard deviation, a_1: lower limit, a_2: upper limit, λ: rate

Name	Description	Units	Prior
Immeabilitas	Imperviousness in %	[-]	LN(38.2,3.82)
Amplitudo	Characteristic Width of the overland flow path	m	LN(900,90)
Affluentia	Baseline Inflow	l/s	LN(3,0.3)
Acclivitas	Catchment Slope in %	[-]	LN(6,0.6)
Longitudo	Conduit Length	m	LN(250,25)
corrlen	Correlation Length of **B** (τ)	min	LN(5,3)
sd.Eps_Q	Standard Deviation of **E** (σ_E)	g(l/s)	LN(0.34,0.034)
sd.B_Q	Standard Deviation of **B** ($\sigma_{B_{ct}}$)	g(l/s)	TN(0,100,0,10^5)
ks_Q	Proportionality Constant between precipitation and uncertainty increase (κ)	g(l/s)·(s/mm)	Exp(10^4)
Delta	Delay between precipitation and uncertainty increase (δ)	[-]	Exp(3)

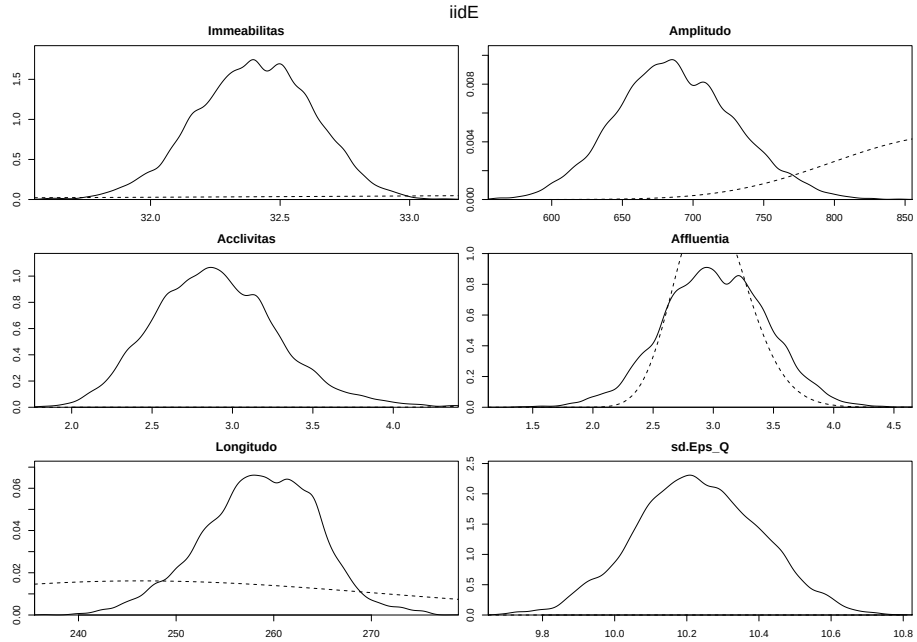

Figure S3: Prior and posterior marginal distributions for $\boldsymbol{\theta}, \boldsymbol{\psi}$ (deterministic model and error model parameters) with the iid untransformed error description. Parameters are described in Tab 1.

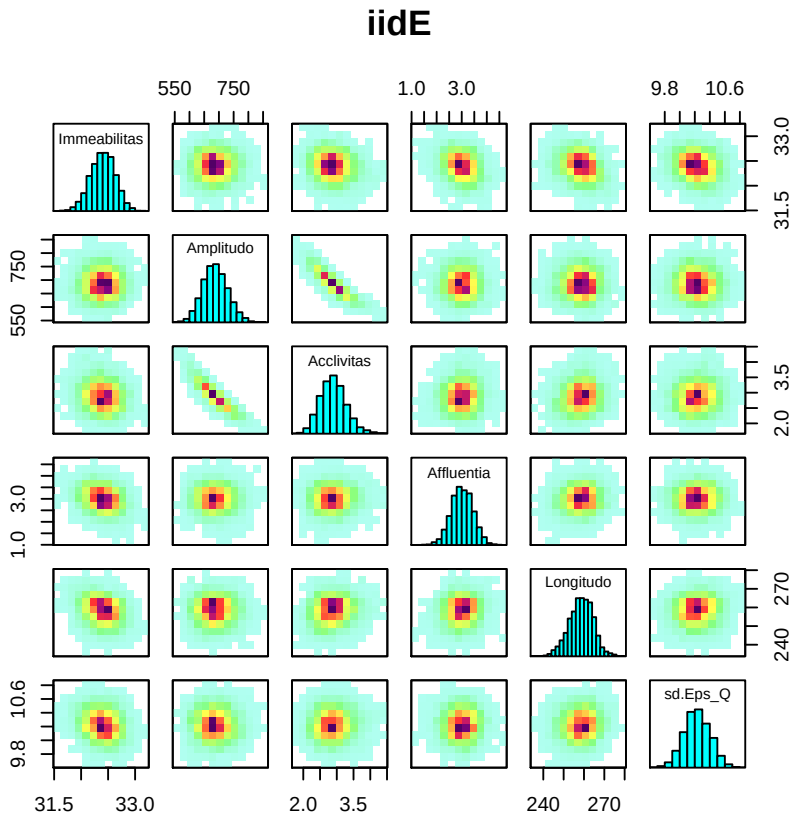

Figure S4: Pairwise scatterplot of posterior marginal distributions for $\boldsymbol{\theta}, \boldsymbol{\psi}$ (deterministic model and error model parameters) with the iid untransformed error description. Parameters are described in Tab 1.

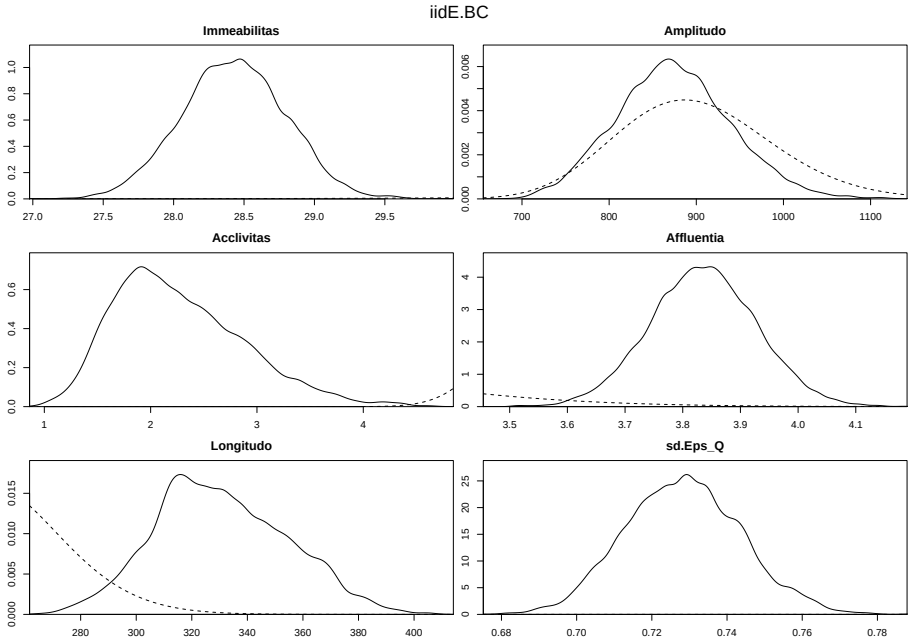

Figure S5: Prior and posterior marginal distributions for $\boldsymbol{\theta}, \boldsymbol{\psi}$ (deterministic model and error model parameters) with the iid Box-Cox transformed error description. Parameters are described in Tab 1.

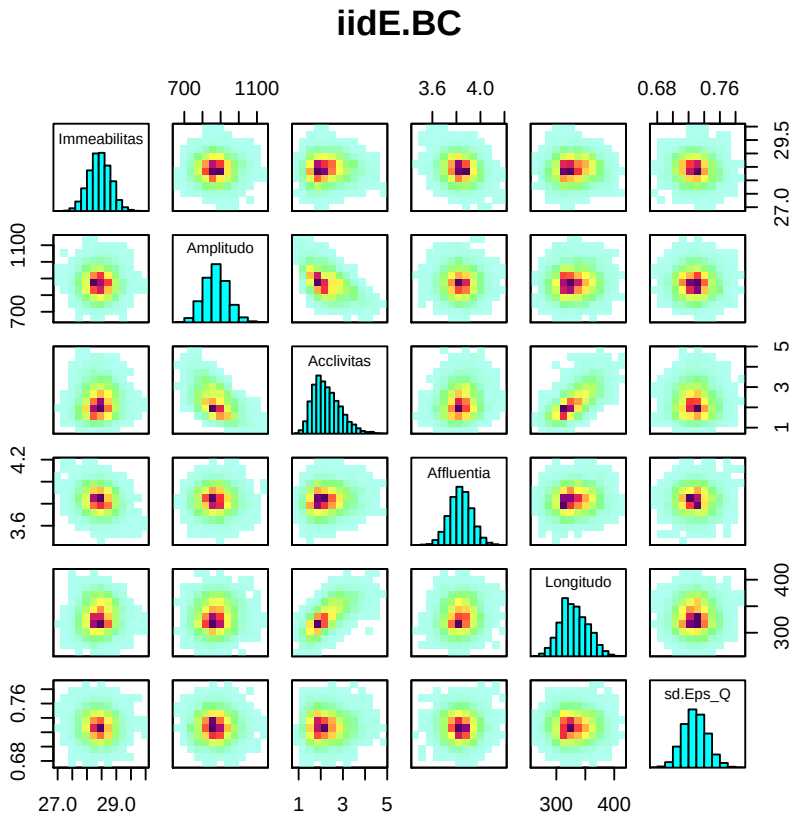

Figure S6: Pairwise scatterplot of posterior marginal distributions for $\boldsymbol{\theta}, \boldsymbol{\psi}$ (deterministic model and error model parameters) with the iid Box-Cox transformed error description. Parameters are described in Tab 1.

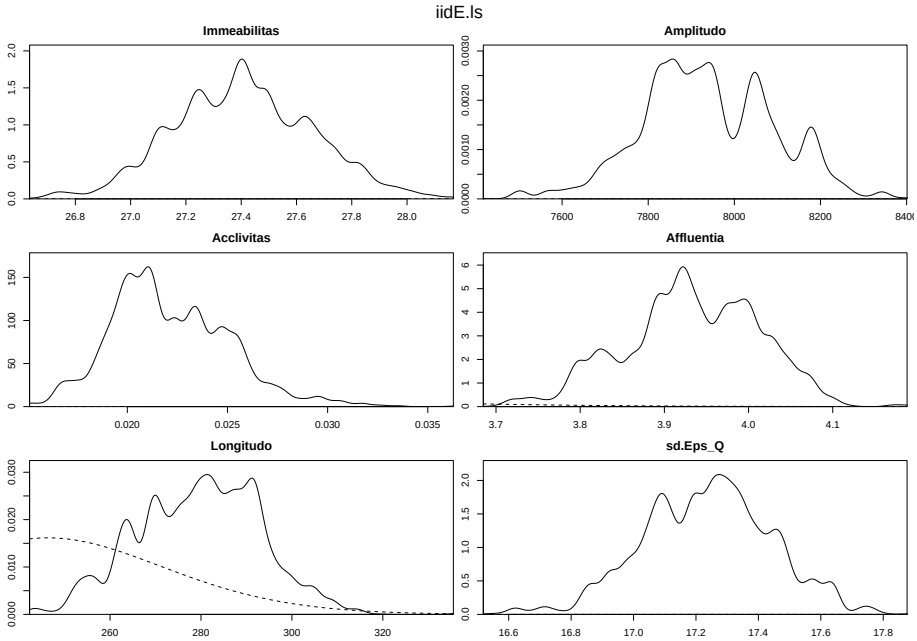

Figure S7: Prior and posterior marginal distributions for $\boldsymbol{\theta}, \boldsymbol{\psi}$ (deterministic model and error model parameters) with the iid log-sinh transformed error description. Parameters are described in Tab 1.

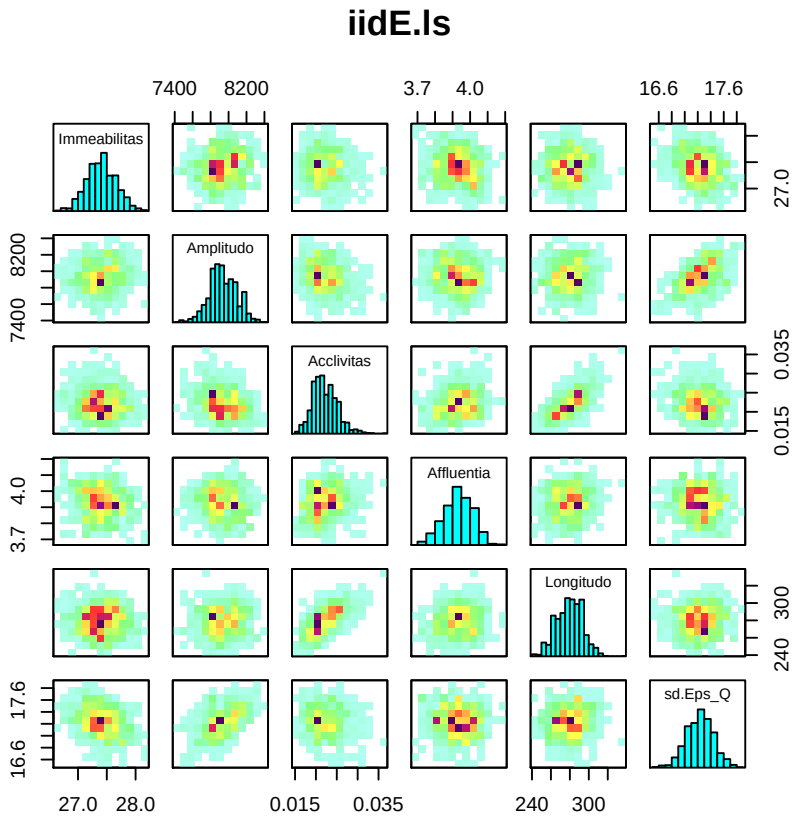

Figure S8: Pairwise scatterplot of posterior marginal distributions for $\boldsymbol{\theta}, \boldsymbol{\psi}$ (deterministic model and error model parameters) with the iid log-sinh transformed error description. Parameters are described in Tab 1.

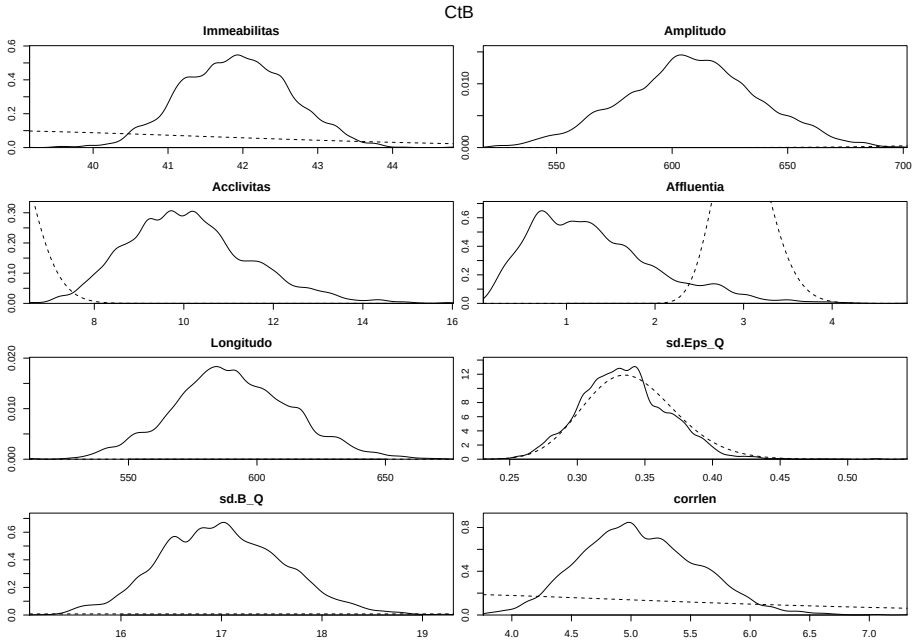

Figure S9: Prior and posterior marginal distributions for $\boldsymbol{\theta}, \boldsymbol{\psi}$ (deterministic model and error model parameters) with the constant untransformed bias description. Parameters are described in Tab 1.

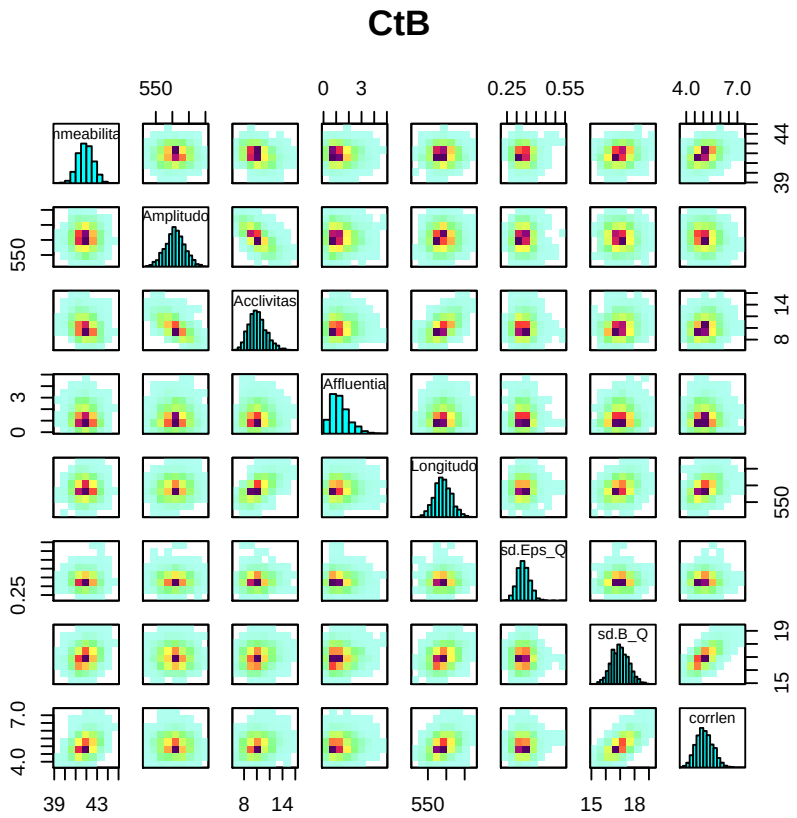

Figure S10: Pairwise scatterplot of posterior marginal distributions for $\boldsymbol{\theta}, \boldsymbol{\psi}$ (deterministic model and error model parameters) with the constant untransformed bias description. Parameters are described in Tab 1.

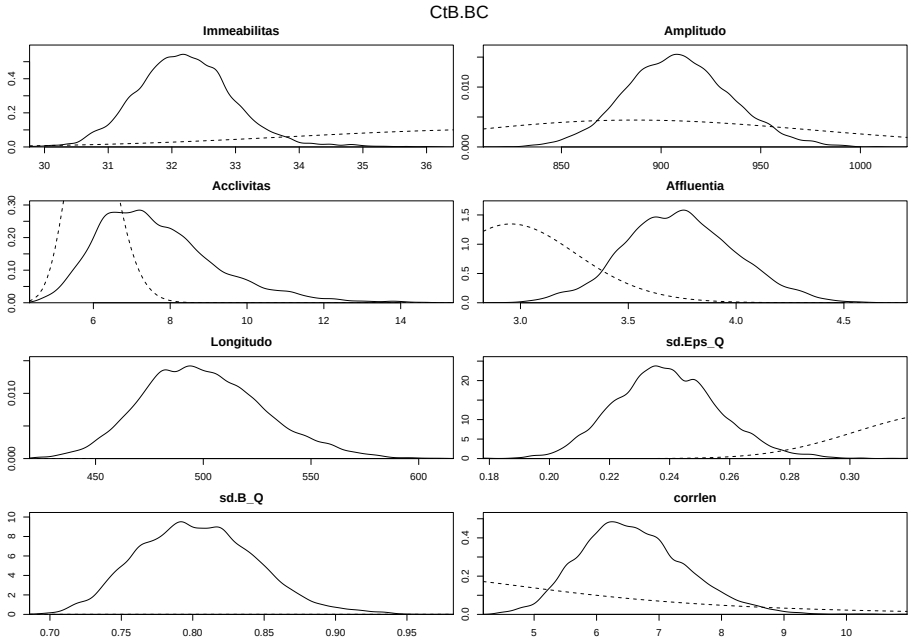

Figure S11: Prior and posterior marginal distributions for $\boldsymbol{\theta}, \boldsymbol{\psi}$ (deterministic model and error model parameters) with the constant Box-Cox transformed bias description. Parameters are described in Tab 1.

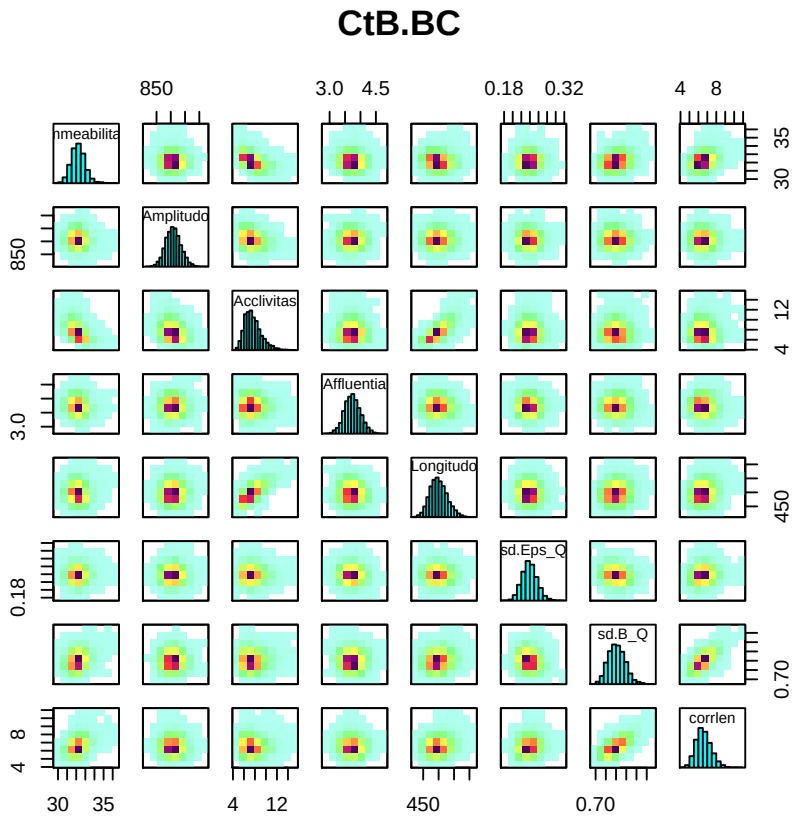

Figure S12: Pairwise scatterplot of posterior marginal distributions for $\boldsymbol{\theta}, \boldsymbol{\psi}$ (deterministic model and error model parameters) with the constant Box-Cox transformed bias description. Parameters are described in Tab 1.

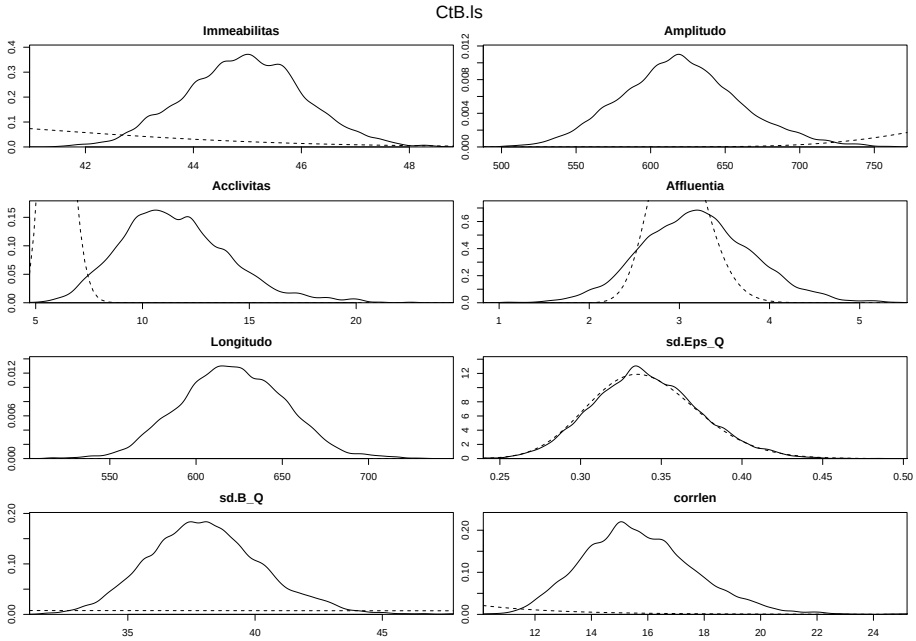

Figure S13: Prior and posterior marginal distributions for $\boldsymbol{\theta}, \boldsymbol{\psi}$ (deterministic model and error model parameters) with the constant log-sinh transformed bias description. Parameters are described in Tab 1.

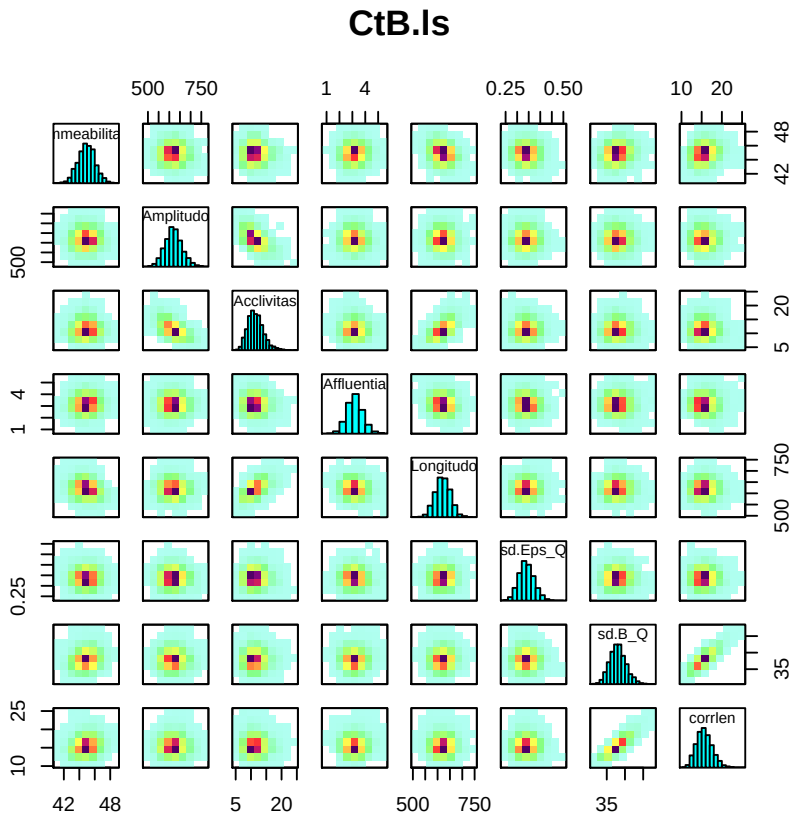

Figure S14: Pairwise scatterplot of posterior marginal distributions for $\boldsymbol{\theta}, \boldsymbol{\psi}$ (deterministic model and error model parameters) with the constant log-sinh transformed bias description. Parameters are described in Tab 1.

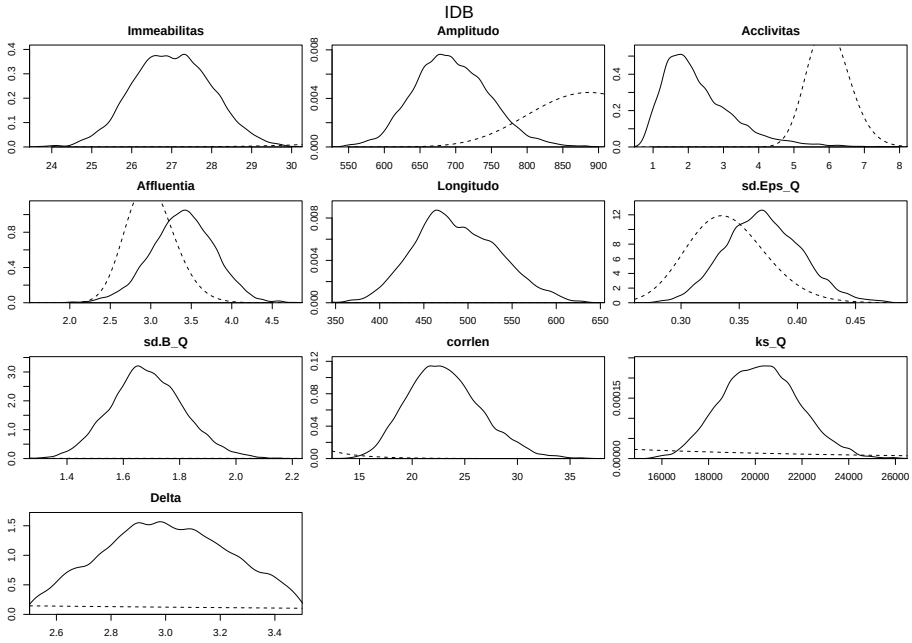

Figure S15: Prior and posterior marginal distributions for $\boldsymbol{\theta}, \boldsymbol{\psi}$ (deterministic model and error model parameters) with the input-dependent untransformed bias description. Parameters are described in Tab 1.

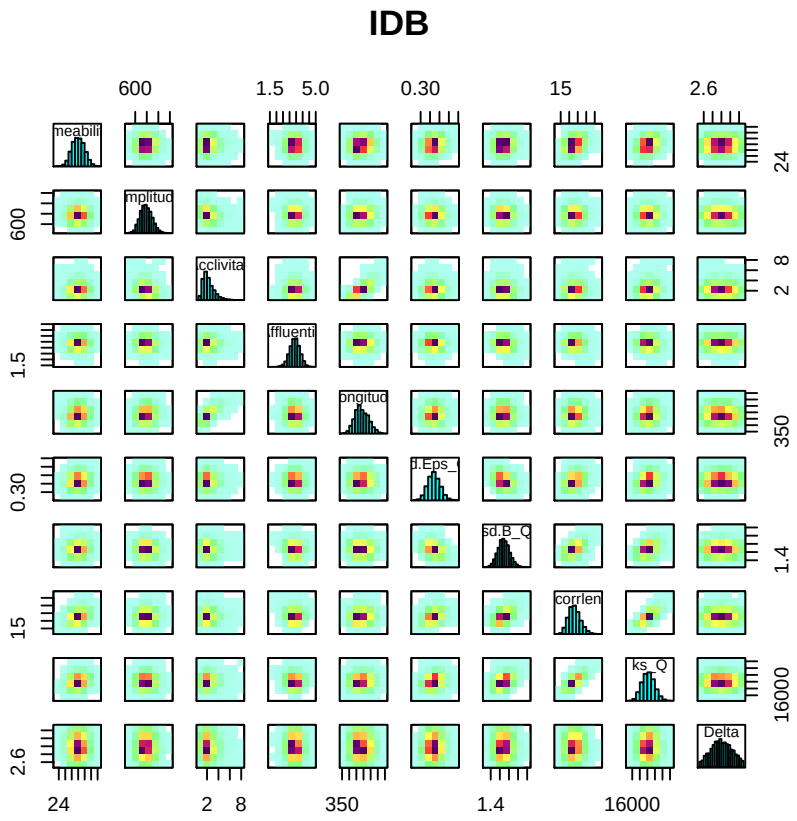

Figure S16: Pairwise scatterplot of posterior marginal distributions for $\boldsymbol{\theta}, \boldsymbol{\psi}$ (deterministic model and error model parameters) with the input-dependent untransformed bias description. Parameters are described in Tab 1.

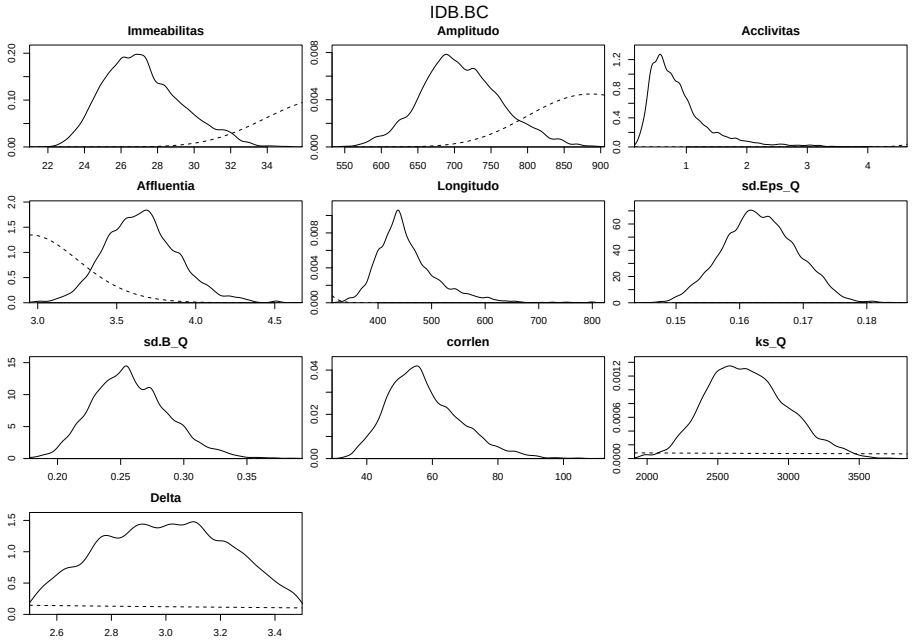

Figure S17: Prior and posterior marginal distributions for $\boldsymbol{\theta}, \boldsymbol{\psi}$ (deterministic model and error model parameters) with the input-dependent Box-Cox transformed bias description. Parameters are described in Tab 1.

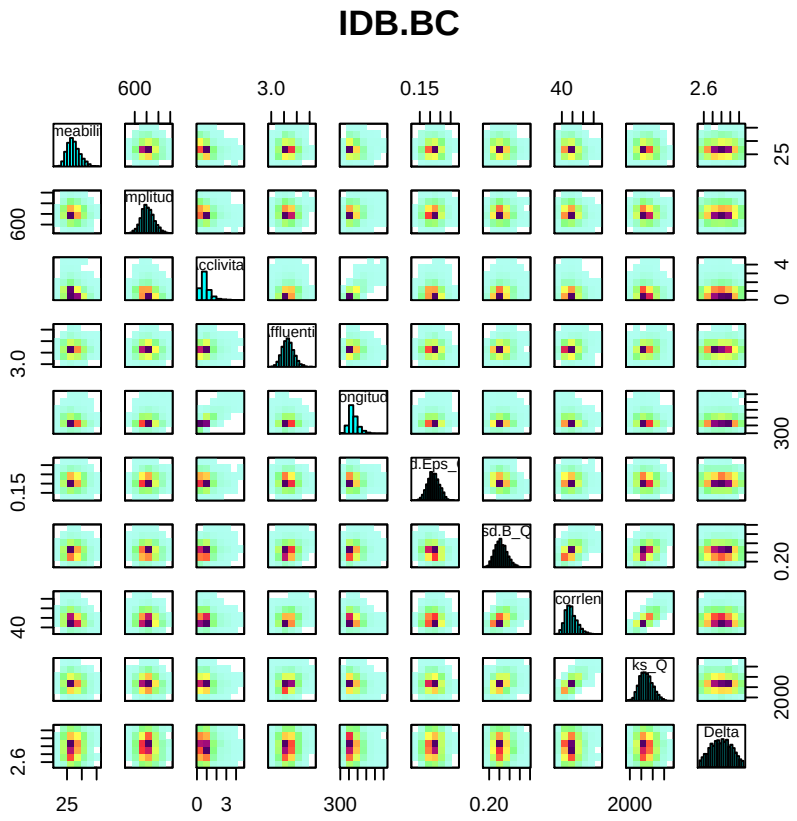

Figure S18: Pairwise scatterplot of posterior marginal distributions for $\boldsymbol{\theta}, \boldsymbol{\psi}$ (deterministic model and error model parameters) with the input-dependent Box-Cox transformed bias description. Parameters are described in Tab 1.

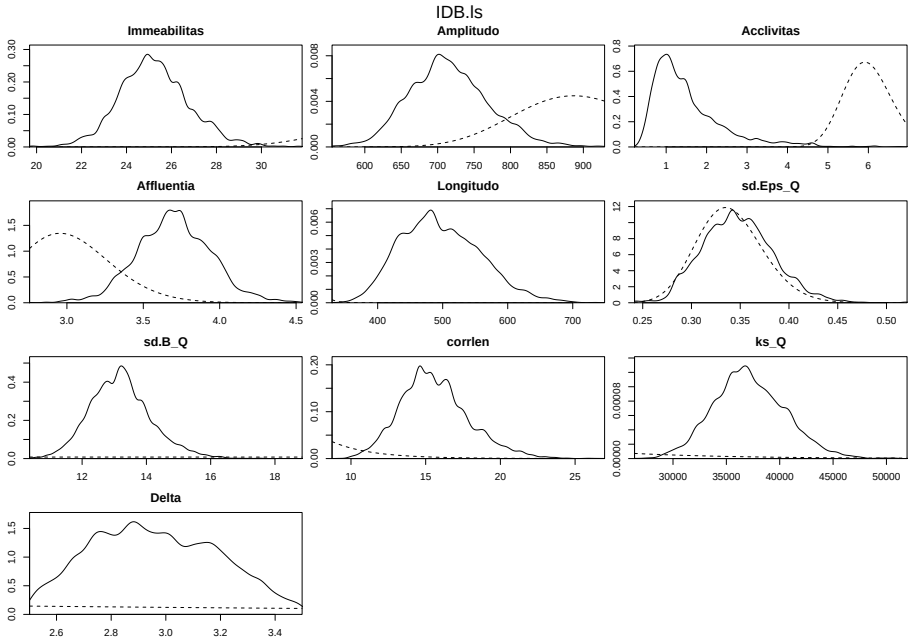

Figure S19: Prior and posterior marginal distributions for $\boldsymbol{\theta}, \boldsymbol{\psi}$ (deterministic model and error model parameters) with the input-dependent log-sinh transformed bias description. Parameters are described in Tab 1.

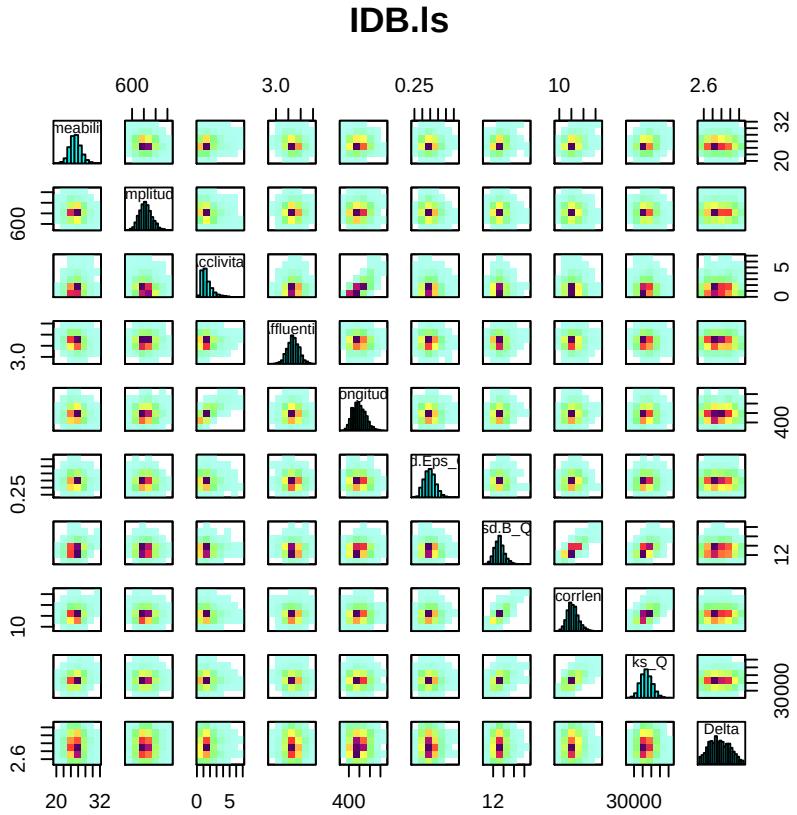

Figure S20: Pairwise scatterplot of posterior marginal distributions for $\boldsymbol{\theta}, \boldsymbol{\psi}$ (deterministic model and error model parameters) with the input-dependent log-sinh transformed bias description. Parameters are described in Tab 1.

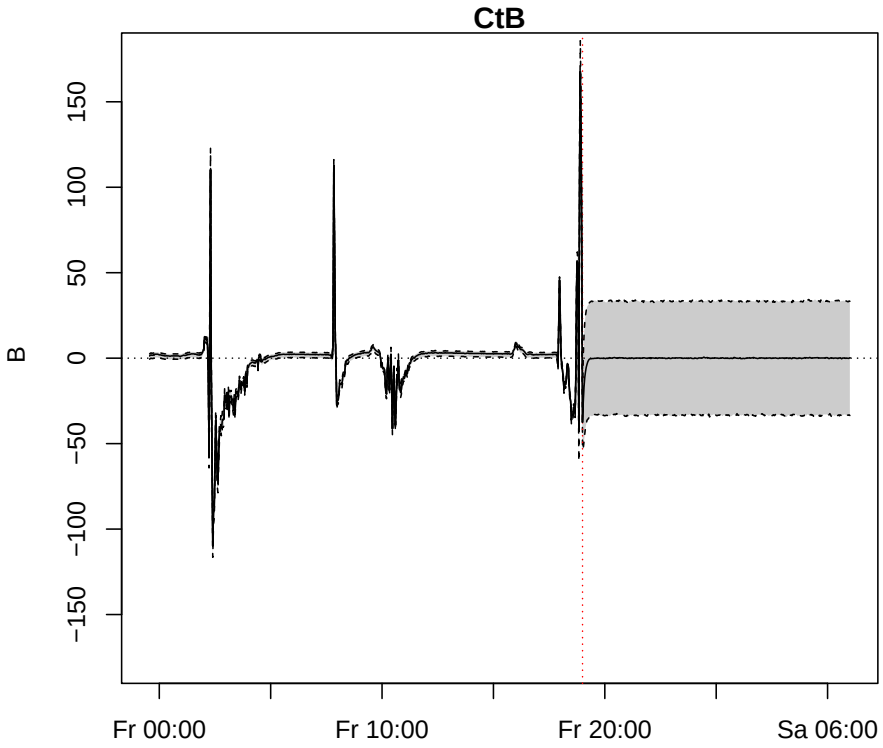

Figure S21: 95% credibility intervals (gray area bounded by dashed lines) and median (solid line) of the bias for part of the calibration (left) and the full validation period (right) obtained with the constant untransformed bias description. The ordinate axis is in transformed flow units. Note that here we do not display the bias-correction but the actual model bias $-\big(\tilde{\mathbf{Y}}_o(\mathbf{x},\boldsymbol{\theta},\boldsymbol{\psi}) - \tilde{\mathbf{y}}_M(\mathbf{x},\boldsymbol{\theta}) - \mathbf{E}(\boldsymbol{\psi})\big)$.

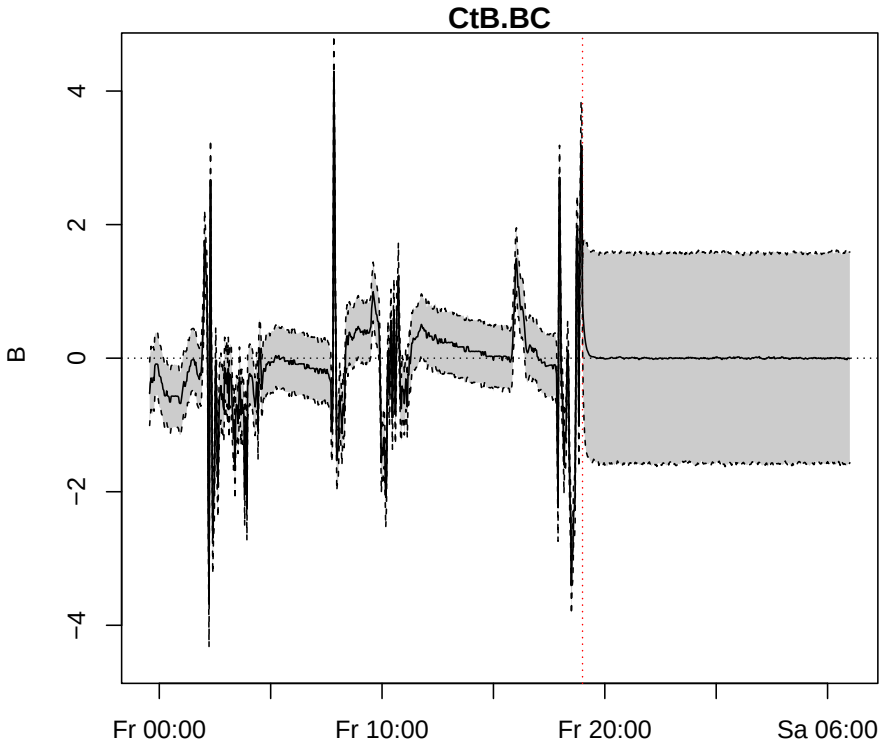

Figure S22: 95% credibility intervals (gray area bounded by dashed lines) and median (solid line) of the bias for part of the calibration (left) and the full validation period (right) obtained with the constant Box-Cox transformed bias description. The ordinate axis is in transformed flow units. Note that here we do not display the bias-correction but the actual model bias $-\big(\tilde{\mathbf{Y}}_o(\mathbf{x},\boldsymbol{\theta},\boldsymbol{\psi}) - \tilde{\mathbf{y}}_M(\mathbf{x},\boldsymbol{\theta}) - \mathbf{E}(\boldsymbol{\psi})\big)$.

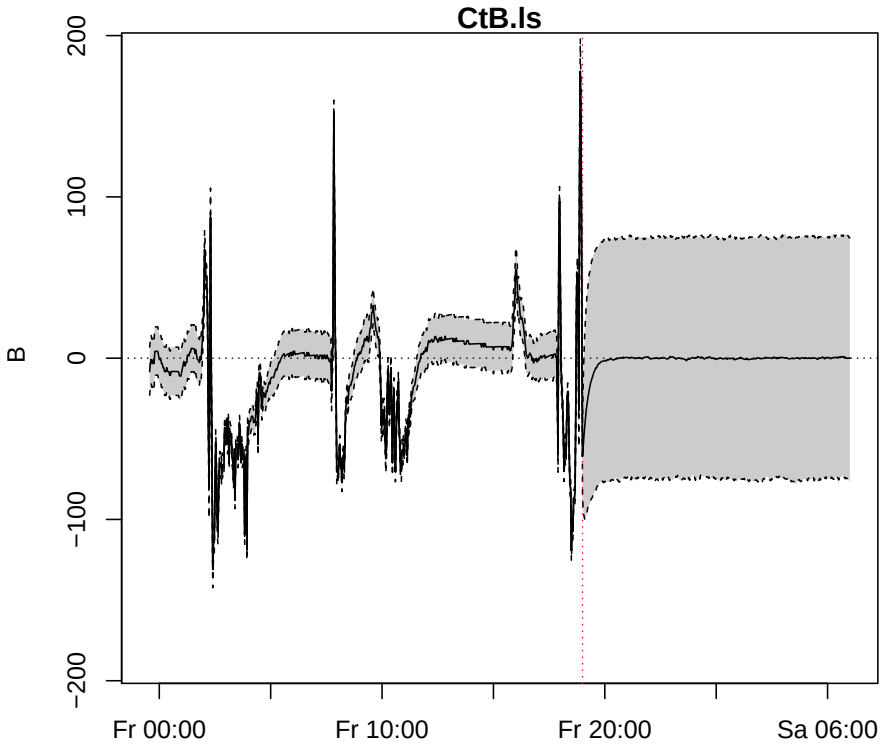

Figure S23: 95% credibility intervals (gray area bounded by dashed lines) and median (solid line) of the bias for part of the calibration (left) and the full validation period (right) obtained with the constant log-sinh transformed bias description. The ordinate axis is in transformed flow units. Note that here we do not display the bias-correction but the actual model bias $-\big(\tilde{\mathbf{Y}}_o(\mathbf{x},\boldsymbol{\theta},\boldsymbol{\psi}) - \tilde{\mathbf{y}}_M(\mathbf{x},\boldsymbol{\theta}) - \mathbf{E}(\boldsymbol{\psi})\big)$.

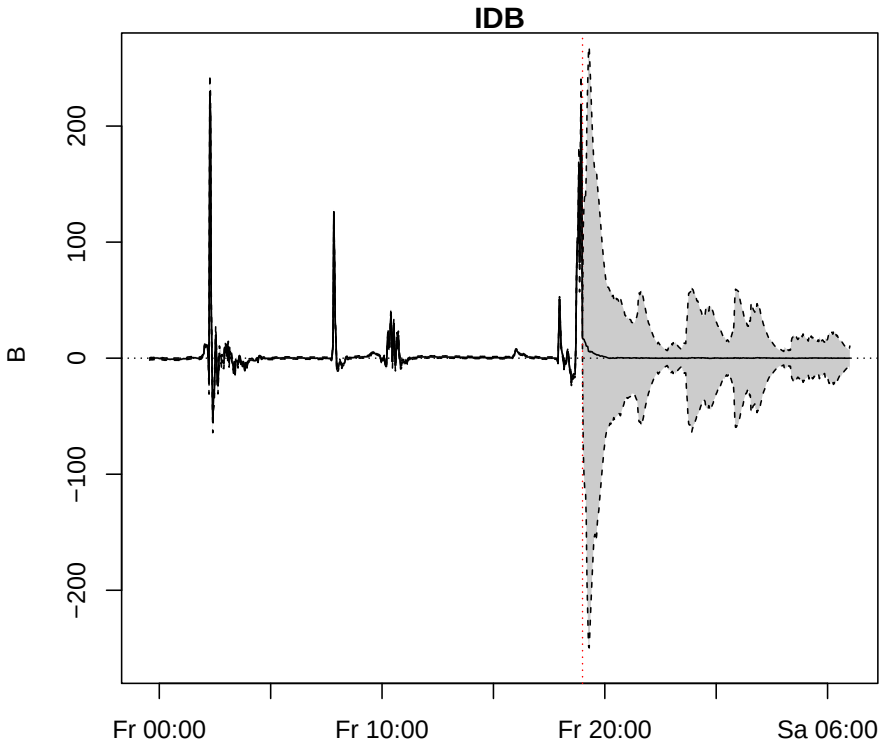

Figure S24: 95% credibility intervals (gray area bounded by dashed lines) and median (solid line) of the bias for part of the calibration (left) and the full validation period (right) obtained with the input-dependent untransformed bias description. The ordinate axis is in transformed flow units. Note that here we do not display the bias-correction but the actual model bias $-\big(\tilde{\mathbf{Y}}_o(\mathbf{x},\boldsymbol{\theta},\boldsymbol{\psi}) - \tilde{\mathbf{y}}_M(\mathbf{x},\boldsymbol{\theta}) - \mathbf{E}(\boldsymbol{\psi})\big)$.

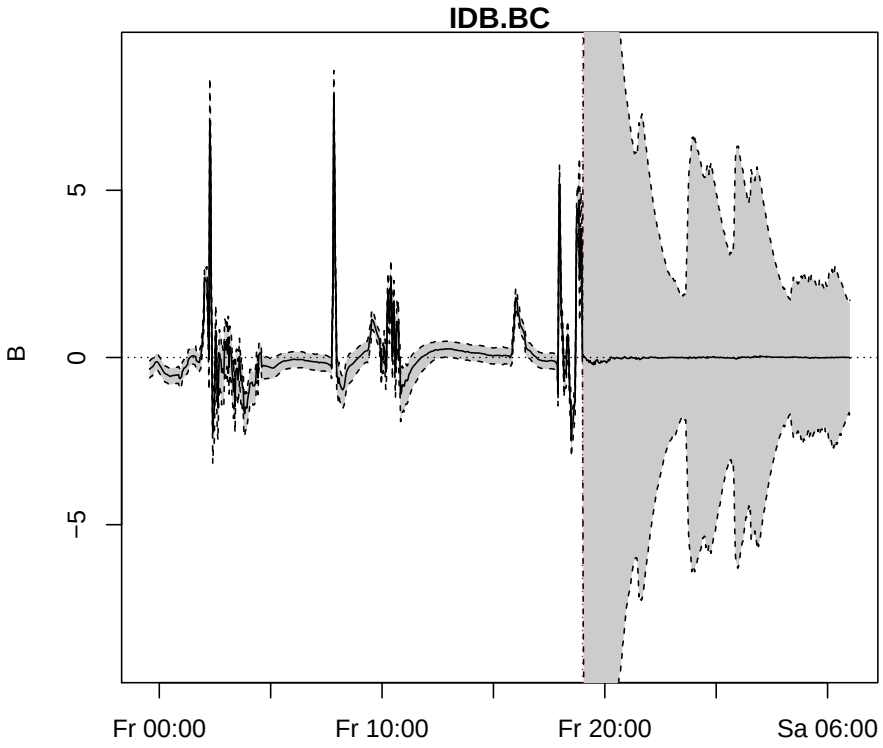

Figure S25: 95% credibility intervals (gray area bounded by dashed lines) and median (solid line) of the bias for part of the calibration (left) and the full validation period (right) obtained with the input-dependent Box-Cox transformed bias description. The ordinate axis is in transformed flow units. Note that here we do not display the bias-correction but the actual model bias $-\big(\tilde{\mathbf{Y}}_o(\mathbf{x},\boldsymbol{\theta},\boldsymbol{\psi}) - \tilde{\mathbf{y}}_M(\mathbf{x},\boldsymbol{\theta}) - \mathbf{E}(\boldsymbol{\psi})\big)$.

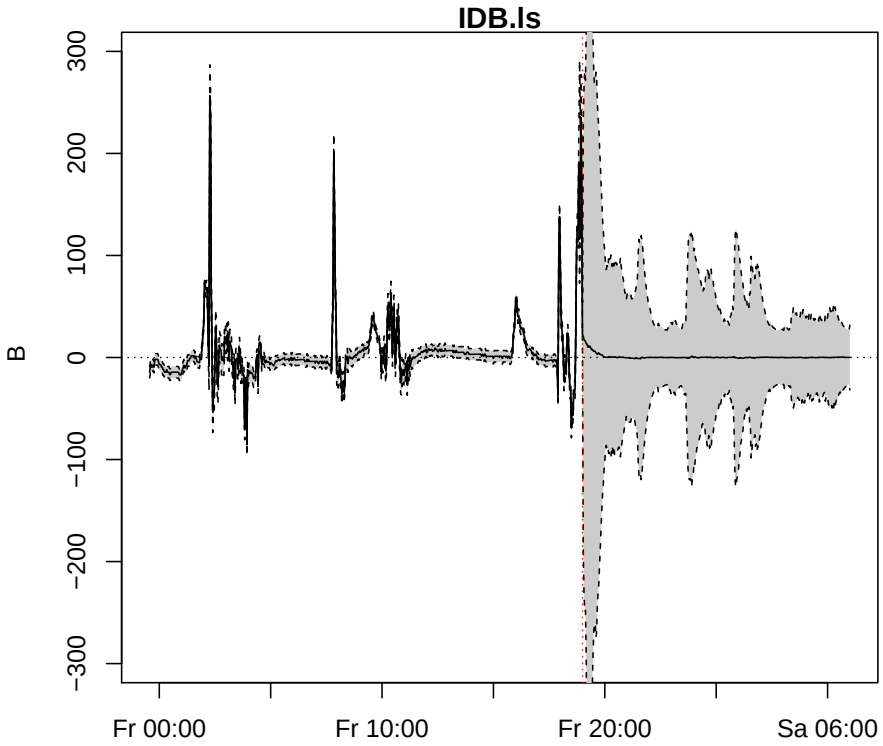

Figure S26: 95% credibility intervalis (gray area bounded by dashed lines) and median (solid line) of the bias for part of the calibration (left) and the full validation period (right) obtained with the input-dependent log-sinh transformed bias description. The ordinate axis is in transformed flow units. Note that here we do not display the bias-correction but the actual model bias $-\big(\tilde{\mathbf{Y}}_o(\mathbf{x},\boldsymbol{\theta},\boldsymbol{\psi}) - \tilde{\mathbf{y}}_M(\mathbf{x},\boldsymbol{\theta}) - \mathbf{E}(\boldsymbol{\psi})\big)$.

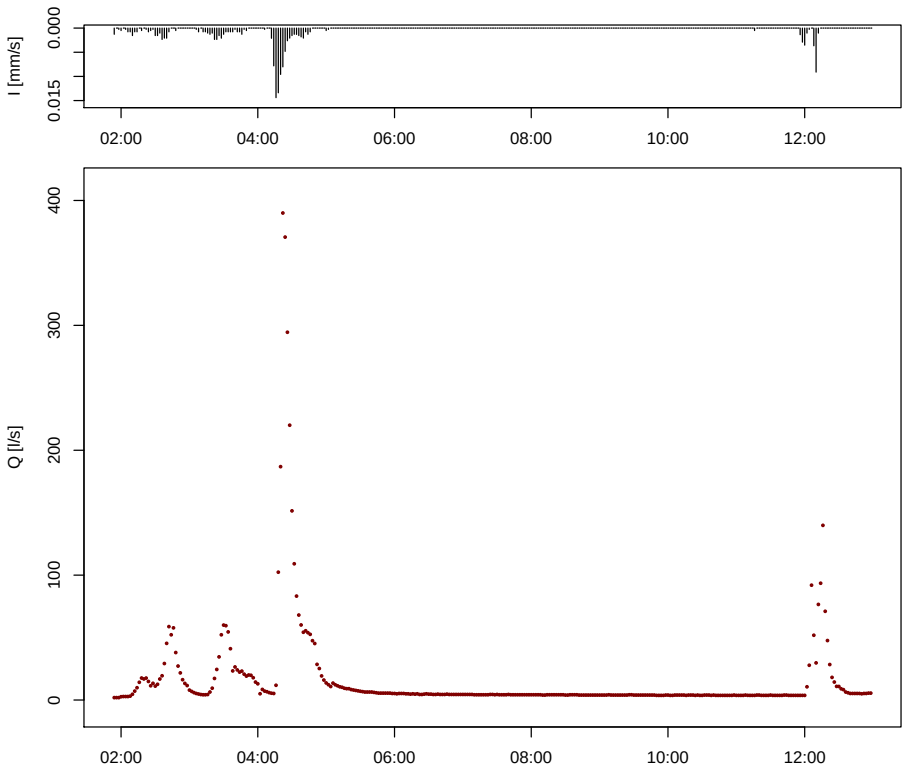

Figure S27: Monitoring data in the calibration period of 27 August.